

Supporting Information

Logic gating of low-abundance molecules using polyelectrolyte-based diodes

Barak Sabbagh, Zhenyu Zhang, and Gilad Yossifon

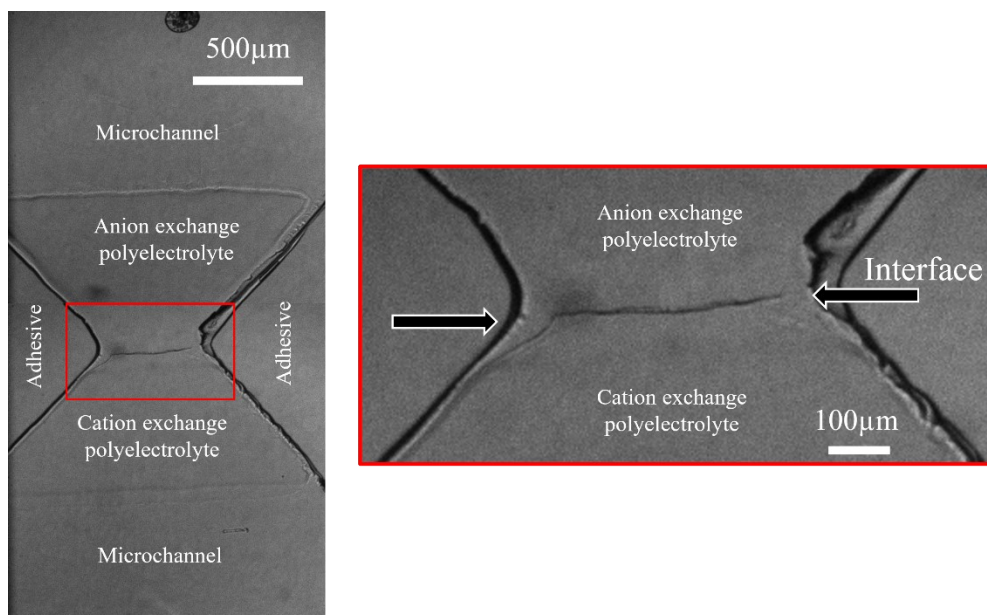


Figure S1: Bright-field microscopy image of a bi-polar diode made of two oppositely charged polyelectrolytes. The image was taken following the sequential introduction of the solution and the polymerization of the polyelectrolytes. A zoom-in image (region marked in red) shows a clear contact line (marked with arrows from both sides) between the anion (top) and cation (bottom) exchange polyelectrolytes along the entire junction.

Fluorescently tagged Dye




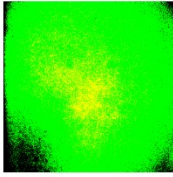
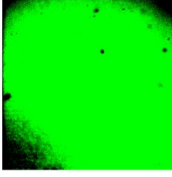
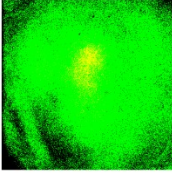
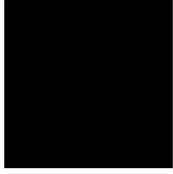

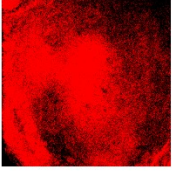
monochromatic laser source Wavelength (nm)	Atto 465 (+)	Alexa 488 (-)	Atto Rho6G (+)
405			
488			
561			

Figure S2: Captured fluorescent intensity for the different fluorescently tagged dyes used in the experiments. Anionic dye (negatively charged): 1 μ M Alexa fluor 488 (middle column) with maximum excitation and emission at a wavelength of 490nm and 525nm, respectively. Cationic dyes (positively charged): 10 μ M Atto 465 (left column) with maximum excitation and emission at a wavelength of 453nm and 505nm, respectively. 5 μ M Atto Rho6G (right column) with maximum excitation and emission at a wavelength of 533nm and 557nm, respectively. All dyes were mixed with a 10mM KCl electrolyte. A quad-band filter with bandwidths of 440,521,607, and 700nm was used to visualize all dyes.

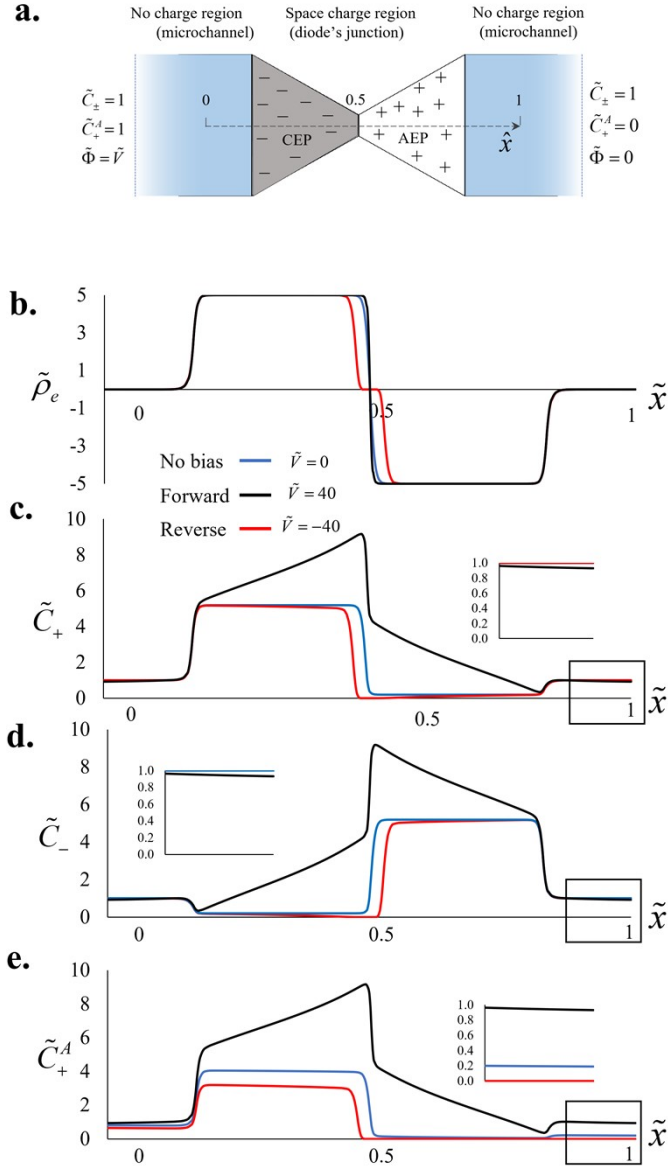


Figure S3: Numerical investigation of the fluidic system containing two oppositely charged polyelectrolytes and interconnecting microchannels on both sides. **a.** schematics of the examined system with the relevant chosen boundary conditions. The normalized steady-state distributions of **b.** the ionic space charge density $\tilde{\rho}_e$, **c.** the concentration of the electrolyte's cations \tilde{c}_+ and **d.** anions \tilde{c}_- , and **e.** the concentration of the cationic analyte \tilde{c}_+^A . Noting that in the studied case, the analyte was initially introduced only to the left reservoir ($\tilde{c}_+^A = 1$), while the right reservoir was kept with zero analyte concentration ($\tilde{c}_+^A = 0$). Only when the diode was forward biased (black line, $V = 40$), the analyte crossed the polyelectrolyte regions.

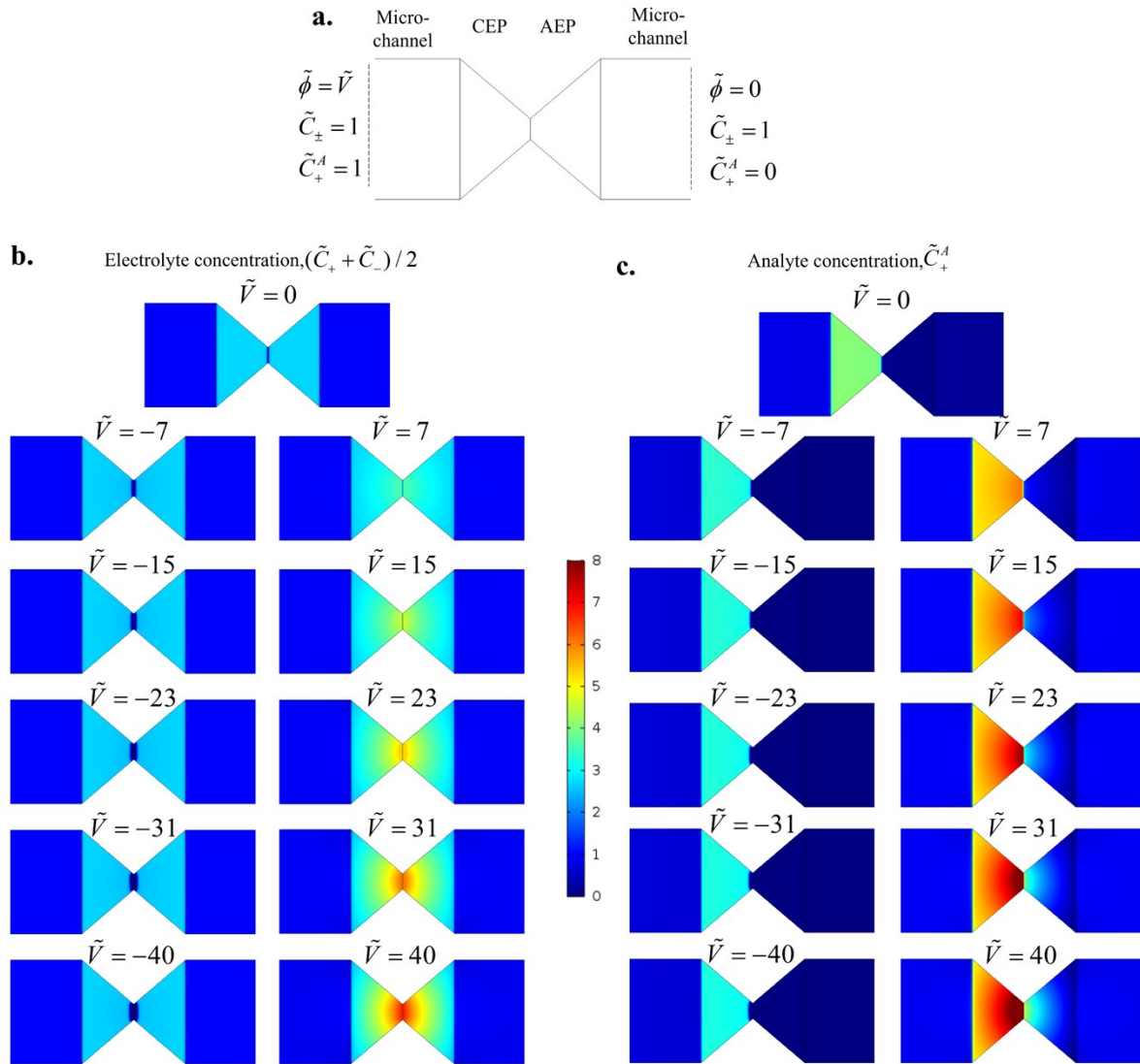


Figure S4: Numerical investigation of the fluidic system containing a diode of anionic and cationic exchange polyelectrolytes (CEP and AEP, respectively) and interconnecting microchannels on both sides. a. schematics of the examined system with the relevant chosen boundary conditions. **b.** The computed electrolyte concentration, $(\tilde{C}_{+} + \tilde{C}_{-})/2$, distribution for various applied potentials of which the diode was reverse biased (i.e., closed, $-40 < \tilde{V} < 0$) and forward biased (i.e., open, $0 < \tilde{V} < 40$). **c.** The computed concentration of a positively charged analyte, \tilde{C}_{+}^A , for the same conditions as **b.**

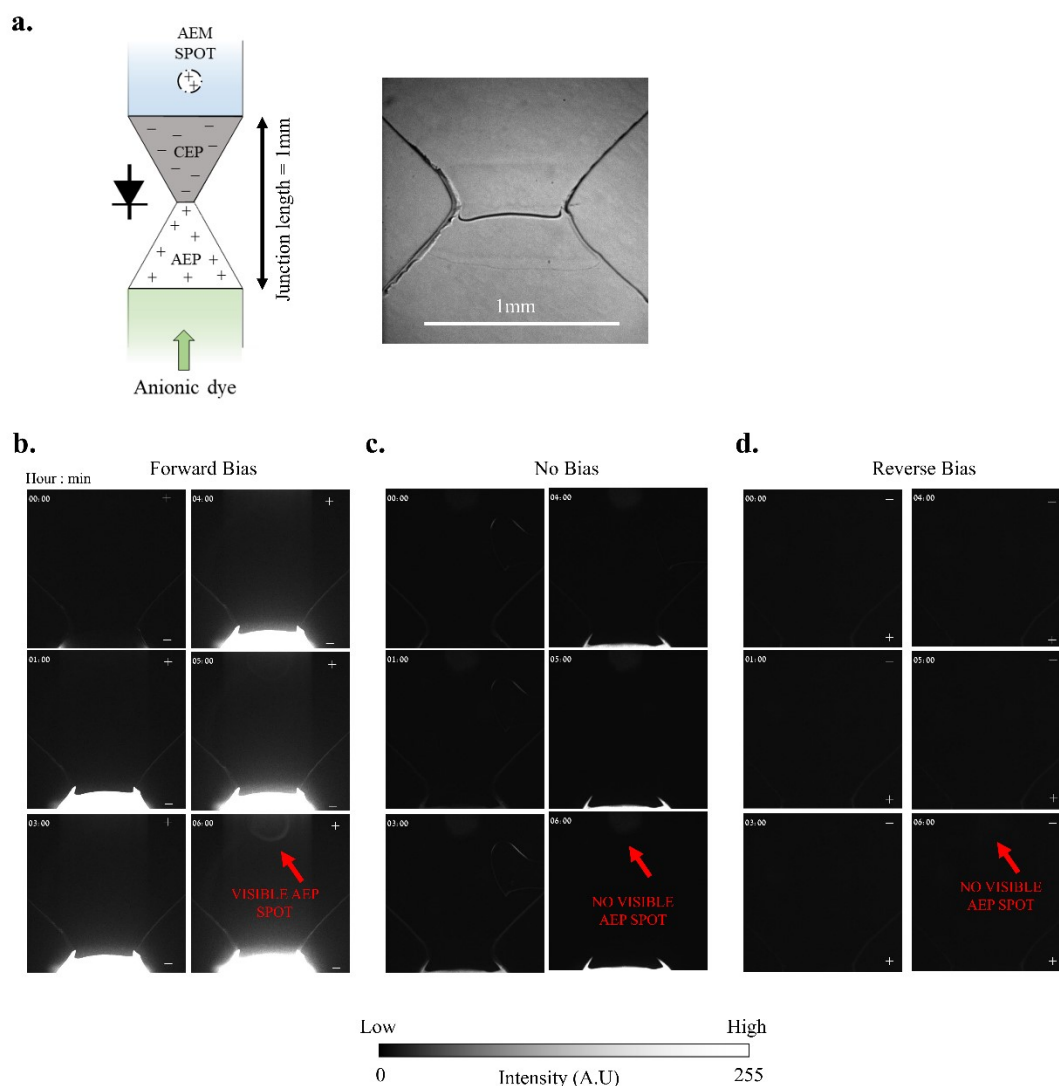


Figure S5: Single-diode gating of anionic analyte: experimental observations for a total ~0.5mm length of the junction. **a.** Schematics of the examined system. A microfluidic system consisting of the bipolar diode (anion and cation exchange polyelectrolytes, AEP and CEP, respectively, total length of ~0.5mm), in addition to an AEP spot to adsorb and accumulate the analyte. Gating was performed for an analyte of 1 μ M negatively charged dye Alexa 488. The analyte was homogeneously mixed within a 10 mM KCl electrolyte solution and initially (t= HH : MM, hour : min) introduced to face the AEP side of the diode (represented by the green arrow), while an electrolyte solution absent of the fluorescent dye was introduced to the CEP side. For each operation mode (**b.:** forward, **c.:** no bias, and **d.:** reverse, corresponding to +1, 0, and -1V, respectively), fluorescence intensity was measured every one hour. A positive indication of the successful passage of the target molecules, in the form of a high-intensity spot, was only obtained after 6h for the forward bias case (compared to >12h operation time for ~2mm junction length).

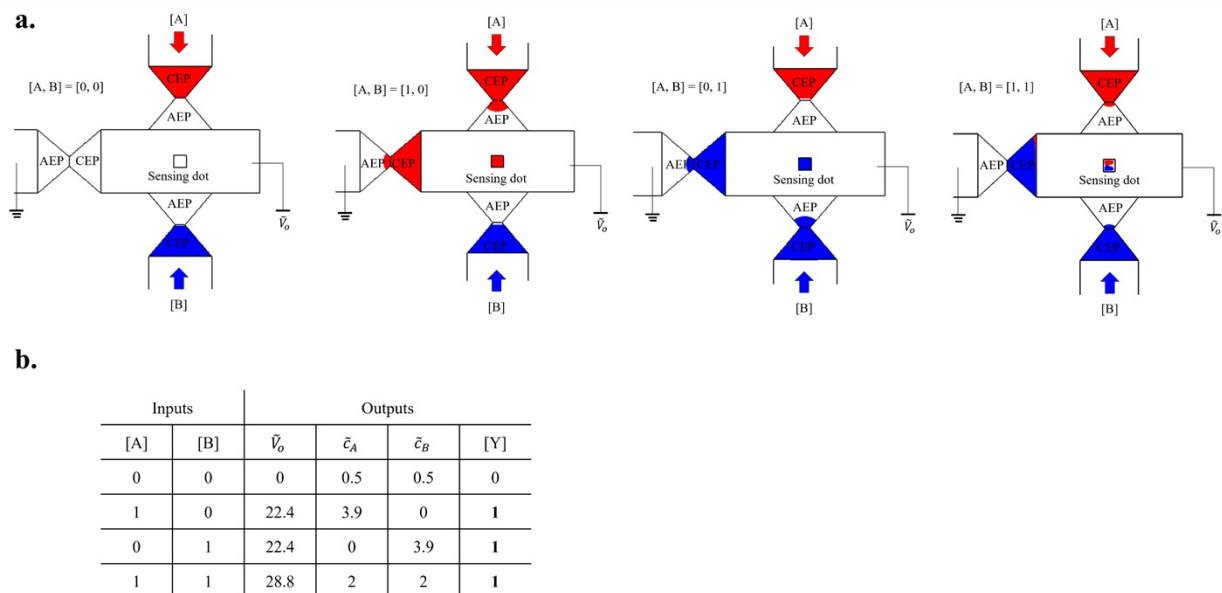


Figure S6: Diode-based OR logic gating of low-abundance molecules: Numerical results. **a.** schematics of the examined fluidic system of ionic OR logic gate. The ionic OR logic gate contained three diodes with two electrical inputs [A], [B] of $\bar{V} = 0$ or 40, corresponding to low ('0') or high ('1') logic input, and an output readout region (V_0). The sensing dot represents a polyelectrolyte spot (see Fig.5) at the readout region (i.e., central microchannel in between all three diodes). At each input, a different cationic analyte was introduced into the inlet reservoir of the corresponding diode (C_A marked in red into input [A], and C_B marked in blue into input [B]). **b.** the calculated open circuit potential, V_0 , and concentration readouts with their associated logic levels ([Y] are summarized in the truth table). A threshold voltage of 20 and a threshold concentration of 2 were set to distinguish the low ('0') and high ('1') logic levels.